Organic Electronics 15 (2014) 3729–3734

Contents lists available at ScienceDirect

Organic Electronics

journal homepage: www.elsevier.com/locate/orgel

Time-independent, high electron mobility in thin $PC_{61}BM$ films: Relevance to organic photovoltaics

A. Devižis [a,b,*], D. Hertel [c], K. Meerholz [c], V. Gulbinas [b], J.-E. Moser [a]

[a] Institute of Chemical Sciences and Engineering, Ecole Polytechnique Fédérale de Lausanne, CH-1015 Lausanne, Switzerland
[b] Center for Physical Sciences and Technology, Savanoriu 231, LT-02300 Vilnius, Lithuania
[c] Department of Chemistry, Physical Chemistry, University of Cologne, Luxemburgerstr. 116, 50939 Cologne, Germany

ARTICLE INFO

Article history:
Received 25 August 2014
Received in revised form 10 October 2014
Accepted 19 October 2014
Available online 30 October 2014

Keywords:
Electroabsorption
Electric field
Ultrafast
Charge carriers
Drift

ABSTRACT

Ultrafast optical probing of electric field by means of electroabsorption combined with conventional photocurrent measurements was employed to investigate the drift and mobility dynamics of photo-generated charge carriers in the pristine $PC_{61}BM$ film and in the blend with a merocyanine dye. Electrons passed a 40 nm thick $PC_{61}BM$ film within a few picoseconds with time-independent and weakly dispersive mobility. The electron mobility is 1 $cm^2/(V\,s)$ at 1 MV/cm and an estimate of the zero-field mobility yields $5 \cdot 10^{-2}$ $cm^2/(V\,s)$. The initial electron mobility in the blend is of the order of 10^{-2} $cm^2/(V\,s)$ and decreases rapidly. We conclude that electron motion in $PC_{61}BM$ based organic bulk hetero-junction solar cells is limited by barriers between $PC_{61}BM$ domains rather than by intrinsic $PC_{61}BM$ properties.

1. Introduction

The opportunity of solution processing and printing is an ultimate advantage of organic photovoltaics (OPV) that assures a low energy investment in the device manufacturing. Most solution processed planar and bulk hetero-junction solar cells rely on the soluble fullerene derivative [6,6]-phenyl-C_{61}-butyric acid methyl ester ($PC_{61}BM$) as an electron acceptor. $PC_{61}BM$ weakly absorbs in the visible range and has poor overlap with the solar-spectrum, thus, weakly contributes to light absorption in $PC_{61}BM$-based solar cells. Attempts to use strongly absorbing polymers [1,2] or small molecules [3] instead of fullerenes resulted in lower performance of devices. Therefore, better understanding of the features, which lie at the heart of success of fullerenes in OPV applications, could help in the development of the competitive acceptor materials and improvement of fullerene based cells.

Charge carrier mobility is one of the crucial parameters for solar cell performance. The mobility is related to the diffusion coefficient by the Einstein relation, thus it characterizes carrier motion. High mobility and, thus, fast diffusion facilitates splitting of the electron–hole pairs at the donor–acceptor interfaces [4–7] and leads to faster extraction of photo-generated charges preventing their accumulation and recombination in the active media of the solar cell. Surprisingly, the electron mobility in $PC_{61}BM$ determined by different methods significantly varies, and actual electron drift and diffusion speed on the length scale typical for solar cells is unknown. Reported electron mobility in $PC_{61}BM$ vary by three to four orders of magnitude. Early work by Mihailetchi et al. reported a value of $2 \cdot 10^{-3}$ $cm^2/(V\,s)$ determined by analysis of space charge limited current (SCLC) [8]. A latter investigation by Tuladhar et al. with the SCLC technique estimated the electron mobility at $(0.8–3.3) \cdot 10^{-2}$ $cm^2/(V\,s)$ in $PC_{61}BM$ films [9]. The electron mobility derived from field-effect transistor operation

* Corresponding author at: Center for Physical Sciences and Technology, Savanoriu 231, LT-02300 Vilnius, Lithuania. Tel.: +370 52644851.
E-mail address: devigy@ar.fi.lt (A. Devižis).

http://dx.doi.org/10.1016/j.orgel.2014.10.028
1566-1199/

also ranges from $4.5 \cdot 10^{-3}$ cm^2/(V s) to $2 \cdot 10^{-1}$ cm^2/(V s) [10–13]. The study of $PC_{61}BM$ microcrystalline powder by pulse-radiolysis time-resolved microwave conductivity provides the sum of electron and hole mobility in the range of $4 \cdot 10^{-2}$–$3 \cdot 10^{-1}$ cm^2/(V s) [14]. This may be considered as being approximately equal to the half of the electron mobility, since the hole mobility in $PC_{61}BM$ is by orders of magnitude lower. The electron mobility of the order of 10^{-1} cm^2/(V s) was obtained in $PC_{61}BM$ domains of PC_{61}-BM/MDMO-PPV blend by means of flash-photolysis time-resolved microwave conductivity technique [15]. An identical mobility value was also estimated from simulation of exciton quenching dynamics in conjugated polymer/PC_{61}-BM blends on the basis of Onsager–Braun model [16]. However, a much lower electron mobility in $PC_{61}BM$ manifold of $3 \cdot 10^{-3}$ cm^2/(V s) was evaluated in recent photoconductivity studies of conjugated polymer APFO-3/$PC_{61}BM$ blends by time-resolved terahertz spectroscopy [17]. Ultrafast Stark-shift spectroscopy was employed by Cabanillas-Gonzalez et al. in order to reveal charge transport in thin $PC_{61}BM$ films [18]. Here, the authors came to the conclusion that the carrier mobility averaged over electrons and holes dropped down from 10^{-1} cm^2/(V s) to 10^{-3}–10^{-4} cm^2/(V s) within 40 ps after photoexcitation. The work was primarily focused on demonstration of the method, therefore some additional effects related to relatively high excitation intensities, which could significantly affect the results, were not analyzed in detail. Thus, despite of numerous investigations, electron mobility values and dynamics in $PC_{61}BM$ and $PC_{61}BM$-based OPV devices remains unclear, preventing clear understanding and modeling of the device performance.

In this work, dynamic Stark shift spectroscopy in combination with photocurrent measurements are employed for the investigation of the charge drift dynamics in thin films of pristine $PC_{61}BM$ and in its blend with merocyanine molecule (MD376/$PC_{61}BM$ blend) [19–21]. We examine the role of charge screening and show that this effect leads to qualitatively different interpretation of the electron mobility dynamics. We conclude that electron mobility is time-independent and weakly dispersive, however, strongly field-dependent in pristine $PC_{61}BM$. On the contrary, the charge mobility is substantially lower and experiences rapid relaxation in blends with organic molecules.

2. Material and methods

Experimental method is based on the measurement of the electric field-induced absorption changes (Stark effect) of organic films sandwiched between semitransparent and metal electrodes. Under reverse bias, when equilibrium carriers are extracted from the active media and their injection is negligible, the material between electrodes behaves like a dielectric medium, and the device resembles a charged capacitor. Under these conditions the applied external bias results in the homogeneously distributed electric field inside the organic layer. Excitation of the film with a short light pulse generates charge carriers, which drift and create counteracting dipoles to the built-in or applied electric field. As a result, initial strength of the electric field decays and electroabsorption (EA) weakens until carriers are extracted from the film. Dynamics of charge drift may be reconstructed from the evolution of the observed EA. More details about the experimental technique may be find elsewhere [18,22].

Experiments were carried out on a typical femtosecond pump–probe setup based on the chirped-pulse amplified Ti:sapphire laser running at the repetition rate of 1 kHz and the output wavelength of 780 nm. Samples were excited at 390 nm utilizing the second harmonic of fundamental radiation. The *p*-polarized white light generated in a sapphire plate was used for probing EA of the samples in reflection configuration (see Supplementary data) at 45 degrees of the incidence angle. Square voltage pulses of reverse bias, synchronized to the laser output and having a duration of about 100 μs were applied to the sample by means of an electrical pulse generator at a frequency of 500 Hz. The measured electromodulated differential absorption (EDA) corresponded to the absorption difference between the biased and unbiased sample at a given probe pulse delay. An oscilloscope was used to measure the photocurrent through a 50 Ω load.

All devices were fabricated on quartz plates sputter-coated with indium–tin oxide (ITO). The substrates were exposed to ozone for 3 min and immediately coated with poly(3,4-ethylene dioxythiophene):poly(styrene sulfonate) (PEDOT:PSS) (HC Starck) and heat treated for 2 min at 110 °C to remove residual water. Before deposition of the active layer, the samples were annealed at 150 °C for 5 min in a nitrogen glove box. Active layers of 40 nm thickness were spin-coated from chlorobenzene solutions of $PC_{61}BM$ and MD376 (15 mg/mL) at 1000 rpm in a nitrogen glove box. For blends, MD376 solution was mixed with $PC_{61}BM$ solution in the 1:1 (w/w) ratio. The device fabrication was completed by thermal evaporation of aluminium.

3. Results and discussion

3.1. Pristine $PC_{61}BM$

Fig. 1 shows EDA spectra of $PC_{61}BM$ film (40 nm) at different delay times. The EDA spectrum at a negative delay time corresponds to the steady state EA, and is in a good agreement with previously published data [23,24]. The electric field in the active media is the sum of the applied field and the built-in field. As determined from photocurrent measurements (not shown), the built-in field approximately equals to 0.2 MV/cm that is in agreement to the work-function difference of the electrodes of 0.8 eV. The insert of Fig. 1 shows the EA amplitude at the peak wavelength of 540 nm versus the square of electric field at the steady-state condition. The linear dependence demonstrates that the amplitude of the EA scales as the square of the field strength, indicating that observed spectral features arise due to the quadratic Stark effect [25–28].

After excitation of $PC_{61}BM$ the EDA amplitude in the observed spectral range starts to decrease without a change in the spectrum. This is evidence of the electric field decay. In general, EDA data may also include a contribution from field-induced changes of the population of

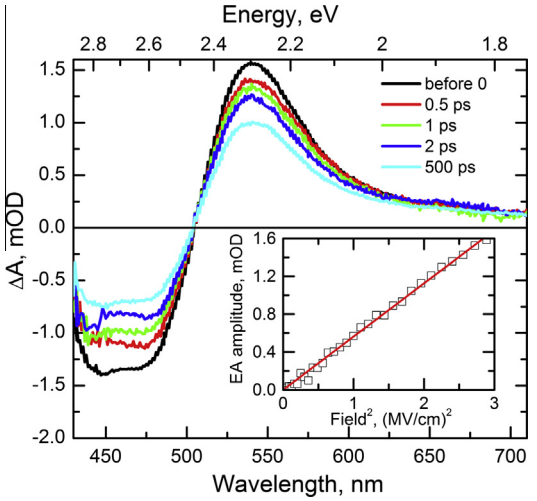

Fig. 1. Electromodulated differential absorption (EDA) spectra of pristine $PC_{61}BM$ film at various delay times (excitation wavelength 390 nm, fluence 2 μJ/cm^2). The applied reverse bias of 6 V corresponds to an electric field intensity of 1.7 MV/cm. Insert shows the electroabsorption amplitude at 540 nm wavelength as a function of the electric field squared.

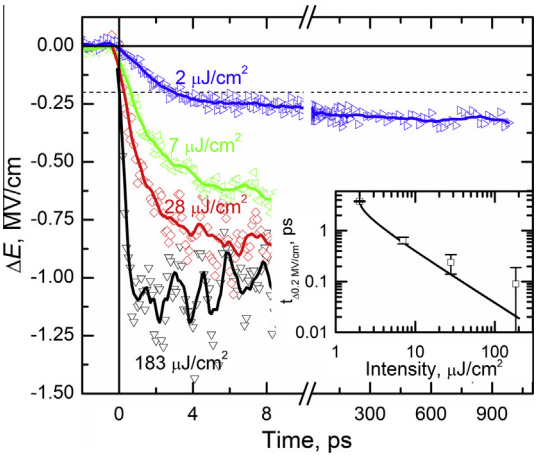

Fig. 2. Change of the electric field as a function of time in pristine $PC_{61}BM$ film under a bias voltage of 6 V (1.7 MV/cm) and excitation fluences of 2 μJ/cm^2, 7 μJ/cm^2 (green), 28 μJ/cm^2 (red) and 183 μJ/cm^2 (black). Insert shows the excitation intensity dependence of the time corresponding to a decrease of the field strength by $\Delta E = -0.2$ MV/cm, points – experimental data, curve plot – extrapolation from low to high intensity according to Eq. (1). (For interpretation of the references to color in this figure legend, the reader is referred to the web version of this article.)

excited state(s). However, absorption of excited states of $PC_{61}BM$ in the visible range is very weak, below 0.1 mOD, at 2 μJ/cm^2 excitation fluence (see Supplementary data). Thus, the field-induced modification of this absorption is certainly much weaker, negligibly contributing to the EDA signal. Therefore, we consider the decay of electric field as the sole cause of the EDA dynamics at the excitation intensity of 2 μJ/cm^2.

The time evolution of EDA kinetics at a peak wavelength of 540 nm were used to reconstruct the evolution of the electric field strength according to the quadratic electroabsorption (EA) dependence on the electric field (insert Fig. 1). Fig. 2 shows the electric field kinetics obtained in $PC_{61}BM$ film with increasing excitation intensity. We note that the field-induced modifications of population density of excited states cannot be neglected at excitation fluences larger than 2 μJ/cm^2. We employed a spectral analysis procedure, which extracts the amplitude of the Stark effect from the EDA data according to the spectral signature of the steady state EA (for more details see Supplementary data). At 2 μJ/cm^2 and 7 μJ/cm^2 excitation intensities, the field kinetics are very similar, the field changes being almost proportional to the excitation intensity. By further increasing excitation intensity the field drop clearly saturates and the shape of the field kinetics change. The space charge screening is the most likely reason for the saturation behavior. This is known from time-of-flight experiments that drifting carriers create a space charge, which reduces and, in the extreme case, eliminates the cause for charge drift – the electric field. It is essential that the drop of the electric field caused by photogenerated charges is much smaller than the applied electric field. This is known as a small charge current (SCC) condition [29]. Disregarding this condition leads to significant errors in carrier mobility and its dynamics. This condition is apparently fulfilled at 2 μJ/cm^2 excitation intensity when the field drop is approximately 5 times lower than the applied field (Fig. 2). A slightly lower increase of the field drop by increasing excitation intensity to 7 μJ/cm^2 shows that the field screening becomes important at this excitation intensity. Thus, in order to avoid distortion of the carrier mobility, the investigations were performed at 2 μJ/cm^2 excitation intensity when concentration of photo-generated charges was low, of about $1.6 \cdot 10^{17}$ cm^{-3} and drifting charges only weakly perturbed the initial field.

The obtained electric field kinetics at different applied voltages are presented in Fig. 3 (data points). The applied field has two consequences: the amplitude of the EA decay increases with the field strength, as does the decay rate. A switchover from a fast decay during initial several ps to a slow decay on a subnanosecond time scale is observed, particularly clearly at 1.2 MV/cm and 1.7 MV/cm field.

Charge carriers are generated very rapidly, within the duration of the excitation pulse in $PC_{61}BM$ [18]. The hole mobility in $PC_{61}BM$ is much lower than the electron mobility [30–32], therefore holes may be considered as being stationary during the extraction time of electrons. This assumption is supported by the fact that the fast decay corresponds to 50% of the total field reduction measured by time-integrated photocurrent, which includes two equal contributions of electrons and holes. Thus, electron motion may be treated separately from the hole motion. In case of prompt carrier generation the photocurrent dynamics is determined by the carrier mobility and their extraction form the sample. In the simplest case, with homogeneous carrier generation and constant electron mobility (meaning that all electrons move at a constant speed determined by the strength of the electric field – $v = \mu \cdot E$), the electron photocurrent should decay only because of the electron extraction. The number of electrons should decrease with time as $1 - v \cdot t/d$, where

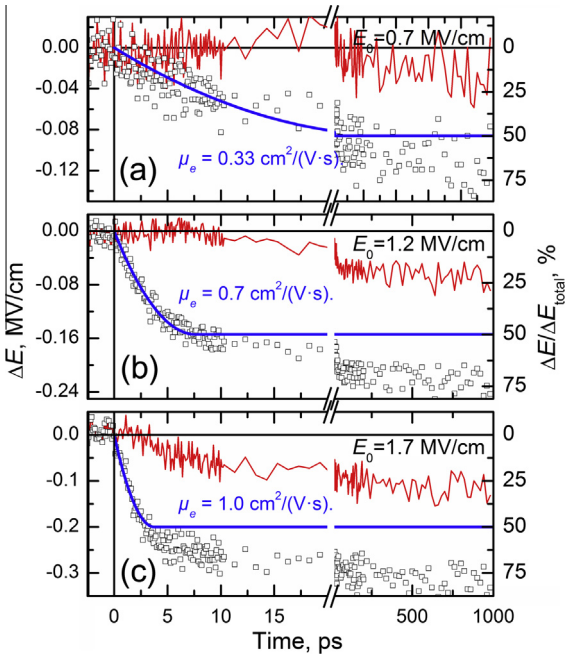

Fig. 3. Change of the electric field (data points) as a function of time in a pristine $PC_{61}BM$ film at various initial electric field strengths (excitation 390 nm, 2 μJ/cm^2). Blue and red lines show electron and hole contributions, respectively (see text for details). (For interpretation of the references to color in this figure legend, the reader is referred to the web version of this article.)

d is the film thickness. Integrating yields a simple parabolic relation for the electric field kinetics during the time of electron extraction:

$$\Delta E(t) = \Delta E_{\text{total}} \frac{1}{t_{\text{drift}}} \cdot \left(t - \frac{t^2}{2 \cdot t_{\text{drift}}} \right). \quad (1)$$

where $t_{\text{drift}} = d/v$ is the drift time, *i.e.* the time needed for electrons to cross the film. The coefficient ΔE_{total} represents the total reduction of the field strength caused by the extraction of all charge carriers.

Relying on the above mentioned assumptions, experimental data shown in Fig. 3 were fitted by Eq. (1) varying only the parameter t_{drift}. We used the time-integrated photocurrent and sample capacitance to calculate ΔE_{total}. The fits closely reproduce the experimental data, especially for a higher applied bias, where the experimental noise is lower. The assumption of the homogeneous excitation over sample thickness is not completely correct because of the considerable optical density of the samples (0.3 OD) at 390 nm excitation wavelength and interference between incident and reflected light. However, our estimations show that accounting for the spatial inhomogeneity would not significantly change the modeling results, the modeled curves would remain within experimental accuracy of the measured kinetics. Amplitudes of fitted curves closely coincide with the end of the fast decay of the electric field. The agreement between the experimental data and fit by Eq. (1) confirms the assumption that the electron mobility is time-independent and weakly dispersive on the given length scale of tens of nanometers. The fit gives the following mobility: 0.33 cm^2/(V s), 0.7 cm^2/(V s) and 1 cm^2/(V s) at field strengths of 0.7 MV/cm, 1.2 MV/cm and 1.7 MV/cm, respectively. Extrapolation of these numbers to zero field by the Poole–Frenkel law – $\mu(E) \sim \mu_0 \exp(\gamma\sqrt{E})$, where γ is the field activation coefficient [33–35], yields a zero-field electron mobility of $5 \cdot 10^{-2}$ cm^2/(V s).

Subtracting the modeled electron contribution from the experimental data, we obtain contributions of holes, shown as red lines in Fig. 3. The extraction of the holes apparently takes place on a nanosecond time scale, suggesting that their mobility is about three orders of magnitude lower than that of electrons.

Additional information about the charge drift may also be obtained from the electric field kinetics at higher excitation intensities, which go beyond the SCC regime. As apparent from Fig. 2, an increase in pump intensity results in a faster decay of the electric field. ΔE_{total} scales linearly with the excitation intensity and leads to a shortening of the time, required to attain a certain reduction of the electric field. Solid curve in the insert of Fig. 2 represents a decay time, corresponding to the reduction of the field by 0.2 MV/cm, extrapolated from 2 μJ/cm^2 to higher intensities according to Eq. (1). Level of $\Delta E = -0.2$ MV/cm is taken as reference and coincides with the complete extraction of electrons within 3.8 ps at 2 μJ/cm^2 excitation intensity. The experimental result at 7 μJ/cm^2 excitation intensity follows the calculated prediction and confirms the time-independent character of the electron drift. The next two data points are limited by time-resolution of the setup but, nevertheless, these points fit to estimated values with a relatively large error margin.

The time-independent electron mobility is in contrast with the results reported in Ref. [18]. The difference is apparently caused by the much higher excitation intensity used in [18], which, as we demonstrated, could cause a significant field screening. Strongly time-dependent carrier mobility was also observed in polymers, where it declined by several orders of magnitude on a ps time scale [36,37] because of the carrier relaxation within the density of states [38]. The absence of such dynamics shows that the energy disorder is less important mobility determining factor in $PC_{61}BM$. Moses et al. demonstrated the temperature-independent photoconductivity in thin films of MEH–PPV and this was related to the carrier extraction prior to the trapping [39]. We suggest that the origin of the time-independent mobility in $PC_{61}BM$ is similar. The length scale of tens of nm is too short for the charges to encounter deep traps, which would lead to the mobility decrease. Likely, the time-dependent mobility in $PC_{61}BM$ would be observed on longer distances. Electron delocalization in the $PC_{61}BM$ microcrystallites on the time-scale of hundreds of fs was proposed in the recent study by Gélinas et al. [7]. However, our data do not show an enhanced mobility at first hundreds of fs. Thus, the delocalization life-time must be too short to have the significant influence on the macroscopic charge transport.

3.2. MD376/$PC_{61}BM$ blend

Electron transport within $PC_{61}BM$ manifold of photovoltaic donor/$PC_{61}BM$ blend may be significantly different

from that of pristine $PC_{61}BM$ due to changes in the composition and morphology of the blend. The same experimental and analysis procedure has been applied for the investigation of the charge transport in typical small molecule/PC_{61}-BM blend. Absorption of MD376 at the 390 nm excitation wavelength is very weak[20], hence $PC_{61}BM$ molecules were predominantly excited, implying that hole transfer from photoexcited $PC_{61}BM$ to MD376 was the main source for carrier generation. The observed electric field decay rate is much slower in the blend than in pristine $PC_{61}BM$ film (insert in Fig. 4). At a low excitation intensity, which corresponds to the SCC regime, the electric field in the blend decays gradually without the clearly noticeable switchover from the fast to slow regime that was observed in pristine $PC_{61}BM$. The difference of the electric field decay rate in comparison with the pristine $PC_{61}BM$ is roughly two orders of magnitude. Apparently, the drift of electrons is impeded in the blend in comparison to pristine $PC_{61}BM$. An increase in the excitation intensity causes similar changes of the field kinetics as in pristine $PC_{61}BM$, but formation of the space charge and, hence, field screening is much slower (see Supplementary data Fig. S3). Kinetics of the electric field in the blend are inconsistent with a time-independent mobility. Fig. 4 presents the running average of the mobility of charge carriers in $PC_{61}BM$/MD376 blend films as a function of time at field strengths of 1.7 MV/cm, 1.2 MV/cm, and 0.7 MV/cm. The running average of the mobility was calculated as the average carrier drift distance divided by the drift time and electric field (see Supplementary data for details). Unlike in pristine $PC_{61}BM$, where the respective contributions of electrons and holes to the charge drift were estimated, owing to a large difference in their mobilities, separation of both contributions in the blend is not possible because the mobility of electrons is apparently comparable to that of holes. Even at early time of a few hundreds of femtoseconds after excitation, the averaged mobility is of the order of 10^{-2} $cm^2/(V\,s)$ in the blend, two orders of magnitude lower than the electron mobility in pristine $PC_{61}BM$. The initial mobility values are more than by one order of magnitude lower than those obtained in annealed P3HT/$PC_{61}BM$ blend [6]. This difference probably arises due to the blend morphology. $PC_{61}BM$ apparently does not form large domains in blends with merocyanines, preventing the formation of a crystalline structure, while in annealed P3HT blends the segregation is clearer. In large $PC_{61}BM$ domains, one may expect similar electron transport as in pristine $PC_{61}BM$, at least initially, until drifting electrons encounter a morphological structure of the donor that is unfavorable for a further electron drift. Comparing electron mobility in pristine film and in blend, we conclude that even at 1:1 (w/w) fullerene concentration, much higher than percolation threshold which is 15 % by volume fraction for $PC_{61}BM$ [30], the electron transport in blends is completely determined by obstacles for electron motion between fullerene domains rather than by the intrinsic mobility in $PC_{61}BM$. The dramatic drop of the electron mobility in blends explains importance of the blend morphology and fullerene concentration for the carrier generation and recombination and consequently for the solar cell performance. This conclusion is in agreement with the fact that efficient solar cells require high fullerene concentration and suggests that improvement of the electron mobility in blends is primarily important in order to achieve high solar cell operation efficiency.

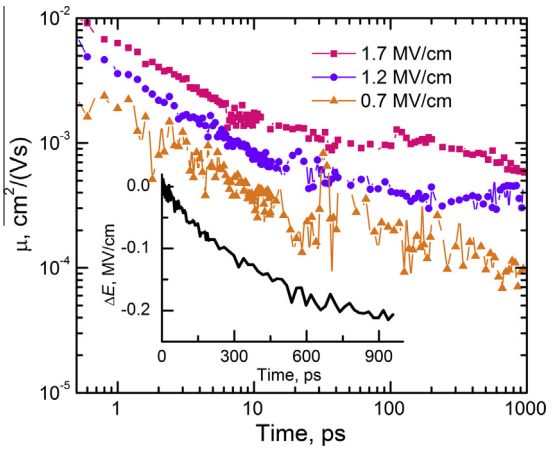

Fig. 4. Kinetics of the running average of the charge carrier mobility in MD376/$PC_{61}BM$ (1:1 w/w) blend device at 6 V (pink), 4 V (violet), and 2 V (orange) applied voltages, obtained by combining measurement results at various excitation intensities (see Supplementary data for details). Insert displays time evolution of the electric field strength under an applied voltage of 6 V (1.7 MV/cm) and excitation fluence of 2 $\mu J/cm^2$. (For interpretation of the references to color in this figure legend, the reader is referred to the web version of this article.)

4. Conclusions

The Stark effect measured by means of the electromodulated differential absorption technique enables detection of the electric field dynamics caused by drift of photogenerated charge carriers in pristine $PC_{61}BM$ and MD376/$PC_{61}BM$ blend films. The field decay in pristine $PC_{61}BM$ film (40 nm thickness) revealed weakly dispersive motion of electrons with the time-independent mobility of about 1 $cm^2/(V\,s)$ at the field strength of 1 MV/cm and estimated zero field mobility of about $5 \cdot 10^{-2}$ $cm^2/(V\,s)$. In contrast, the average charge carrier mobility in MD376/$PC_{61}BM$ (1:1 w/w) blend is time-dependent and decays from about 10^{-2} $cm^2/(V\,s)$ to 10^{-4} $cm^2/(V\,s)$ within one nanosecond at the field strength of 1 MV/cm. A much slower electron drift in MD376/$PC_{61}BM$ (1:1 w/w) blend, with respect to pristine $PC_{61}BM$ film, indicates that the blend film morphology is unfavorable for charge transport. This suggests that $PC_{61}BM$ domains are absent or very small.

Acknowledgments

This work was partly funded by the scientific exchange programme between Switzerland and the new member states of the European Union (Sciex-NMS^{ch} Project No. 12.059). We would like to acknowledge Prof. F. Würthner (Universität Würzburg) for the supply of the merocyanine dye and Stefan Röllgen (Köln) for sputtering ITO on quartz. DH and KM thank the German BMBF (FKZ 03EK3503C) for financial support. AD and JEM are grateful to the Swiss National Science Foundation and NCCR-MUST for funding.

Appendix A. Supplementary material

Supplementary data associated with this article can be found, in the online version, at http://dx.doi.org/10.1016/j.orgel.2014.10.028.

References

[1] X. Zhan, Z.A. Tan, B. Domercq, Z. An, X. Zhang, S. Barlow, Y. Li, D. Zhu, B. Kippelen, S.R. Marder, A high-mobility electron-transport polymer with broad absorption and its use in field-effect transistors and all-polymer solar cells, J. Am. Chem. Soc. 129 (23) (2007) 7246–7247.

[2] X. Zhan, Z.A. Tan, E. Zhou, Y. Li, R. Misra, A. Grant, B. Domercq, X-H Zhang, Z. An, X. Zhang, et al., Copolymers of Perylene Diimide with dithienothiophene and dithienopyrrole as electron-transport materials for all-polymer solar cells and field-effect transistors, J. Mater. Chem. 19 (32) (2009) 5794–5803.

[3] P.E. Schwenn, K. Gui, A.M. Nardes, K.B. Krueger, K.H. Lee, K. Mutkins, H. Rubinstein-Dunlop, P.E. Shaw, N. Kopidakis, P.L. Burn, et al., A small molecule non-fullerene electron acceptor for organic solar cells, Adv. Energy Mater. 1 (1) (2011) 73–81.

[4] A.A. Bakulin, A. Rao, V.G. Pavelyev, P.H. van Loosdrecht, M.S. Pshenichnikov, D. Niedzialek, J. Cornil, D. Beljonne, R.H. Friend, The role of driving energy and delocalized states for charge separation in organic semiconductors, Science 335 (6074) (2012) 1340–1344.

[5] C.S. Ponseca Jr., A. Yartsev, E Wang, M.R. Andersson, D. Vithanage, V. Sundström, Ultrafast terahertz photoconductivity of bulk heterojunction materials reveals high carrier mobility up to nanosecond time scale, J. Am. Chem. Soc. 134 (29) (2012) 11836–11839.

[6] D.A. Vithanage, A. Devižis, V. Abramavičius, Y. Infahsaeng, D. Abramavičius, R.C.I. MacKenzie, P.E. Keivanidis, A. Yartsev, D. Hertel, J. Nelson, et al., Visualizing charge separation in bulk heterojunction organic solar cells, Nat. Commun. 4 (2013), http://dx.doi.org/10.1038/ncomms3334.

[7] S. Gélinas, A. Rao, A. Kumar, S.L. Smith, A.W. Chin, J. Clark, T.S. van der Poll, G.C. Bazan, R.H. Friend, Ultrafast long-range charge separation in organic semiconductor photovoltaic diodes, Science 343 (6170) (2014) 512–516.

[8] V.D. Mihailetchi, J.K. van Duren, P.W. Blom, J.C. Hummelen, R.A. Janssen, J.M. Kroon, M.T. Rispens, W.J.H. Verhees, M.M. Wienk, Electron transport in a methanofullerene, Adv. Funct. Mater. 13 (1) (2003) 43–46.

[9] S.M. Tuladhar, D. Poplavskyy, S.A. Choulis, J.R. Durrant, D.D. Bradley, J. Nelson, Ambipolar charge transport in films of methanofullerene and poly (phenylenevinylene)/methanofullerene bends, Adv. Funct. Mater. 15 (7) (2005) 1171–1182.

[10] T.D. Anthopoulos, C. Tanase, S. Setayesh, E.J. Meijer, J.C. Hummelen, P.W. Blom, D.M. de Leeuw, Ambipolar organic field-effect transistors based on a solution-processed methanofullerene, Adv. Mater. 16 (23–24) (2004) 2174–2179.

[11] C. Waldauf, P. Schilinsky, M. Perisutti, J. Hauch, C.J. Brabec, Solution-processed organic n-type thin-film transistors, Adv. Mater. 15 (24) (2003) 2084–2088.

[12] E.J. Meijer, D.M. de Leeuw, S. Setayesh, E. Van Veenendaal, B.H. Huisman, P.W.M. Blom, J.C. Hummelen, U. Scherf, T.M. Klapwijk, Solution-processed ambipolar organic field-effect transistors and inverters, Nat. Mater. 2 (10) (2003) 678–682.

[13] T.B. Singh, N. Marjanovic, G.J. Matt, N.S. Sariciftci, R. Schwodiauer, S. Bauer, Nonvolatile organic field-effect transistor memory element with a polymeric gate electret, Appl. Phys. Lett. 85 (22) (2004) 5409–5411.

[14] M.P. de Haas, J.M. Warman, T.D. Anthopoulos, D.M. de Leeuw, The mobility and decay kinetics of charge carriers in pulse-ionized microcrystalline PCBM powder, Adv. Funct. Mater. 16 (17) (2006) 2274–2280.

[15] T.J. Savenije, J.E. Kroeze, M.M. Wienk, J.M. Kroon, J.M. Warman, Mobility and decay kinetics of charge carriers in photoexcited PCBM/PPV blends, Phys. Rev. B 69 (15) (2004) 155205.

[16] D. Veldman, O. Ipek, S.C. Meskers, J. Sweelssen, M.M. Koetse, S.C. Veenstra, J.M. Kroon, S.S. van Bavel, J. Loos, R.A. Janssen, Compositional and electric field dependence of the dissociation of charge transfer excitons in alternating polyfluorene copolymer/fullerene blends, J. Am. Chem. Soc. 130 (24) (2008) 7721–7735.

[17] C.S. Ponseca Jr., H. Němec, N. Vukmirović, S. Fusco, E. Wang, M.R. Andersson, P. Chabera, A. Yartsev, V. Sundström, Electron and hole contributions to the terahertz photoconductivity of a conjugated polymer: fullerene blend identified, J. Phys. Chem. Lett. 3 (17) (2003) 2442–2446.

[18] J. Cabanillas-Gonzalez, T. Virgili, A. Gambetta, G. Lanzani, T.D. Anthopoulos, D.M. de Leeuw, Photoinduced transient stark spectroscopy in organic semiconductors: a method for charge mobility determination in the picosecond regime, Phys. Rev. Lett. 96 (10) (2006) 106601.

[19] N.M. Kronenberg, V. Steinmann, H. Bürckstümmer, J. Hwang, D. Hertel, F. Würthner, K. Meerholz, Direct comparison of highly efficient solution-and vacuum-processed organic solar cells based on merocyanine dyes, Adv. Mater. 22 (37) (2010) 4193–4197.

[20] D. Peckus, A. Devižis, R. Augulis, S. Graf, D. Hertel, K. Meerholz, V. Gulbinas, Charge transfer states in merocyanine neat films and its blends with [6,6]-phenyl-C_{61}-butyric acid methyl ester, J. Phys. Chem. C 117 (12) (2013) 6039–6048.

[21] V. Steinmann, N.M. Kronenberg, M.R. Lenze, S.M. Graf, D. Hertel, H. Bürckstümmer, F. Würthner, K. Meerholz, A simple merocyanine tandem solar cell with extraordinarily high open-circuit voltage, Appl. Phys. Lett. 99 (19) (2011) 193306.

[22] V. Gulbinas, R. Kananavičius, L. Valkunas, H. Bässler, Dynamic stark effect as a probe of the evolution of geminate electron-hole pairs in a conjugated polymer, Phys. Rev. B 66 (23) (2002) 233203.

[23] T. Drori, C.X. Sheng, A. Ndobe, S. Singh, J. Holt, Z.V. Vardeny, Below-gap excitation of π-conjugated polymer-fullerene blends: implications for bulk organic heterojunction solar cells, Phys. Rev. Lett. 101 (3) (2008) 037401.

[24] T. Drori, J. Holt, Z.Y. Vardeny, Optical studies of the charge transfer complex in polythiophene/fullerene blends for organic photovoltaic applications, Phys. Rev. B 82 (7) (2010) 075207.

[25] M. Liess, S. Jeglinski, Z.V. Vardeny, M. Ozaki, K. Yoshino, Y. Ding, T. Barton, Electroabsorption spectroscopy of luminescent and nonluminescent π-conjugated polymers, Phys. Rev. B 56 (24) (1997) 15712.

[26] M. Tong, C.X. Sheng, Z.V. Vardeny, Nonlinear optical spectroscopy of excited states in polyfluorene, Phys. Rev. B 75 (12) (2007) 125207.

[27] M.G. Harrison, S. Möller, G. Weiser, G. Urbasch, R.F. Mahrt, H. Bässler, U. Scherf, Electro-optical studies of a soluble conjugated polymer with particularly low intrachain disorder, Phys. Rev. B 60 (12) (1999) 8650.

[28] G. Weiser, A. Horvath, Variation with disorder of absorption and electroabsorption spectra of a π-conjugated polymer: 4BCMU, Chem. Phys. 227 (1) (1998) 153–166.

[29] A. Pivrikas, N.S. Sariciftci, G. Juška, R.A. Österbacka, Review of charge transport and recombination in polymer/fullerene organic solar cells, Prog. Photovolt: Res. Appl. 15 (8) (2007) 677–696.

[30] K. Vakhshouri, D.R. Kozub, C. Wang, A. Salleo, E.D. Gomez, Effect of miscibility and percolation on electron transport in amorphous poly (3-hexylthiophene)/phenyl-C 61-butyric acid methyl ester blends, Phys. Rev. Lett. 108 (2) (2012) 026601.

[31] H. Morishita, W.J. Baker, D.P. Waters, R. Baarda, J.M. Lupton, C. Boehme, Mechanisms of spin-dependent dark conductivity in films of a soluble fullerene derivative under bipolar injection, Phys. Rev. B 89 (12) (2014) 125311.

[32] R. Könenkamp, G. Priebe, B. Pietzak, Carrier mobilities and influence of oxygen in C 60 films, Phys. Rev. B 60 (16) (1999) 11804.

[33] J. Frenkel, On pre-breakdown phenomena in insulators and electronic semi-conductors, Phys. Rev. 54 (8) (1938) 647.

[34] H. Bässler, Charge transport in disordered organic photoconductors a Monte Carlo simulation study, Phys. Status Solidi (B) 175 (1) (1993) 15–56.

[35] P.W.M. Blom, M.J.M. De Jong, M.G. Van Munster, Electric-field and temperature dependence of the hole mobility in poly (p-phenylene vinylene), Phys. Rev. B 55 (2) (1997) R656.

[36] E. Hendry, M. Koeberg, J.M. Schins, H.K. Nienhuys, V. Sundström, L.D.A. Siebbeles, M. Bonn, Interchain effects in the ultrafast photophysics of a semiconducting polymer: THz time-domain spectroscopy of thin films and isolated chains in solution, Phys. Rev. B 71 (12) (2005) 125201.

[37] C.H. Lee, G. Yu, D. Moses, A.J. Heeger, Picosecond transient photoconductivity in poly (p-phenylenevinylene), Phys. Rev. B 49 (4) (1994) 2396.

[38] A. Devižis, A. Serbenta, K. Meerholz, D. Hertel, V. Gulbinas, Ultrafast dynamics of carrier mobility in a conjugated polymer probed at molecular and microscopic length scales, Phys. Rev. Lett. 103 (2) (2009) 027404.

[39] D. Moses, J. Wang, G. Yu, A.J. Heeger, Temperature-independent photoconductivity in thin films of semiconducting polymers: photocarrier sweep-out prior to deep trapping, Phys. Rev. Lett. 80 (12) (1998) 2685.